J Appl Electrochem (2009) 39:1993–1999
DOI 10.1007/s10800-009-9909-z

ORIGINAL PAPER

Electrochemical oxidation of perfluorobutane sulfonate using boron-doped diamond film electrodes

Zhaohui Liao · James Farrell

Received: 2 December 2008 / Accepted: 14 April 2009 / Published online: 30 April 2009

Abstract This research investigated oxidation of perfluorobutane sulfonate (PFBS) at a boron-doped diamond (BDD) film anode. PFBS oxidation produced carbon dioxide, sulfate, fluoride, and trace amounts of trifluoroacetic acid (TFA). Rate constants for PFBS oxidation as a function of current density and temperature were measured using a rotating disk electrode (RDE) reactor. Reaction rates in the RDE reactor were zeroth order with respect to PFBS concentration, which is indicative of a reaction limited by the availability of reactive sites. The apparent electron transfer coefficient and apparent activation energy were used to evaluate the rate-limiting step for PFBS oxidation. Density functional simulations were used to calculate the reaction energies and activation barriers for PFBS oxidation by hydroxyl radicals and by direct electron transfer. Simulation results indicated that the experiments were performed at sufficiently high overpotentials that the rate-limiting step was an activationless direct electron transfer reaction.

Keywords Perfluorooctane sulfonate · Oxidation · Boron-doped diamond · Density functional theory

1 Introduction

Perfluoroalkyl sulfonate (PFAS) compounds are widely used in semiconductor manufacturing. The most commonly used PFAS compound in the electronics industry is perfluorooctyl sulfonate (PFOS). Studies conducted in the late 1990s have shown that PFOS bioaccummulates in humans, fish, and other animals [1]. The American Red Cross reported a mean PFOS serum level of 34.9 μg L^{-1} in donated blood, and mean serum levels in other countries have been found to range from 17 to 53 μg L^{-1} [2]. PFOS does not break down in the environment and has an elimination half-life of 4 years in the human body [2].

Because of PFOS accumulation in the environment, the United State Environmental Protection Agency (EPA) and several European governments have banned the use of PFOS [3, 4]. Most replacements for PFOS are shorter chain length PFAS compounds, with perfluorobutane sulfonate (PFBS) being the most widely used. Although PFBS has smaller bioconcentration factors than PFOS, it still accumulates in the environment and is nonbiodegradable.

Currently, there are no effective treatment methods for the destructive removal of PFBS or any other PFAS compounds from wastewater streams. Conventional destructive treatment via advanced oxidation processes (AOPs) is ineffective for PFAS oxidation because the carbon–fluorine bonds in PFAS are very stable and do not react with the hydroxyl radicals produced in conventional AOPs [5]. The ineffectiveness of conventional AOPs necessitates new technologies for the destructive removal of PFAS compounds from water.

The aim of this research was to investigate the oxidative removal of PFBS from aqueous solutions using anodes composed of boron-doped diamond (BDD) films on p-silicon substrates. Toward that end, reaction rates for PFBS at BDD anodes were determined over a range of electrode potentials, current densities, and temperatures. Density functional theory (DFT) simulations were then used to evaluate possible reaction mechanisms.

Z. Liao · J. Farrell (✉)
Department of Chemical and Environmental Engineering, University of Arizona, Tucson, AZ 85721, USA
e-mail: farrellj@email.arizona.edu

2 Materials and methods

2.1 Rotating disk electrode reactor

Experiments measuring PFBS reaction rates were performed in 10 mM sodium perchlorate background electrolyte solutions with initial pH values of 5.0 in custom-made glass reaction cells with volumes of 350 or 600 mL. Sodium perchlorate was selected as the electrolyte because previous studies have shown that perchlorate is not oxidized at BDD anodes [6]. An initial PFBS concentration of 0.4 mM was used in all experiments. A circulating water bath was used to control the temperature to within ±0.2 °C and experiments were performed at temperatures ranging from 7 to 45 °C. The working electrode consisted of a BDD film coated on a 1.13 cm diameter p-silicon disk (Adamant Technologies, Neuchatel, Switzerland) contained within a Princeton Applied Research (PAR) (Oak Ridge, TN) model 616 rotating disk electrode (RDE) holder. In order to eliminate the effect of diffusive mass transfer limitations on the measured reaction rates, the disk electrode was rotated at a speed of 3,000 revolutions per minute (rpm). A 0.3-mm diameter by 16-cm long platinum wire (Aesar, Ward Hill, MA) was used as the counter electrode, and a PAR Hg/Hg_2SO_4 electrode was used as the reference. Electrode potentials and currents were controlled using a PAR model 273A potentiostat. All potentials were corrected for uncompensated solution resistance and reported with respect to the standard hydrogen electrode (SHE). Because the RDE reactor was open to the atmosphere through the electrode shaft opening, the loss of volatile reaction products could not be prevented. Therefore, the reaction products were determined in experiments performed in a gas-tight, closed-loop, flow-through reactor.

2.2 Flow-through reactor

A MiniDiacell® (Adamant Technologies) flow-through reactor containing two monopolar and one bipolar BDD films on p-silicon electrodes was used to perform a mass balance on the reactants and products. Two 5-cm long by 2.5-cm wide monopolar electrodes were connected to the power supply as anode and cathode. A bipolar electrode of the same dimensions was held between the anode and cathode with an interelectrode gap of 0.3 cm. There was no reference electrode and the cell was operated galvanostatically using a direct current power supply. The total anode surface area of 25 cm^2 and the void volume of 15 mL yielded a surface area to solution volume ratio of 1.67 $cm^2\ mL^{-1}$. The closed-loop, flow-through system consisted of a 2.5-L liquid chromatography reservoir and liquid chromatography pump connected to the electrode reactor with 0.32 cm outer diameter (o.d.) Teflon® tubing. The fluid reservoir was instrumented with a pressure gauge connected via a 15-cm long by 0.635-cm o.d. stainless steel column containing a palladium catalyst (Aldrich). The catalyst served to promote O_2 and H_2 recombination into water, thereby preventing excessive pressure build-up from the gas production accompanying water electrolysis. The closed-loop system was tested to be gas tight over the pressure range of the experiments. Experiments were performed by placing 1 L of 0.4 mM PFBS in 10 mM $NaClO_4$ into the feed water reservoir. During the electrolysis experiments, the solution was pumped through the reactor at a flow rate of 10.0 mL min^{-1} and periodically sampled for PFBS and product concentrations. In order to account for only the time that each fluid element in the closed-loop system was in the reactor and subject to electrolysis, the electrolysis times were calculated according to:

$$\text{electrolysis time} = \text{elapsed real time} \times \frac{\text{reactorvolume}}{\text{total fluid volume in the closed loop}}. \quad (1)$$

2.3 Product analyses

Perfluorobutane sulfonate concentrations were determined by analyses of diluted aqueous samples using a Dionex ICS-3000 ion chromatograph (IC) equipped with an autosampler, an Acclaim Polar Advantage II C18 column (4.6 × 250 mm), and an electrical conductivity detector. The mobile phase consisted of acetonitrile and water containing a 20 mM borate buffer at a pH value of 8. Fluoride, sulfate, and TFA concentrations were determined by analyses of diluted aqueous samples using a Dionex DX 500 IC equipped with an autosampler, an Ionpac As11-HC anion-exchange column (4 × 250 mm), and an electrical conductivity detector. The eluent was 12 mM potassium hydroxide. Gas and aqueous phase products from the flow-through reactor were analyzed by the Mass Spectrometry Facility in the Department of Chemistry at University of Arizona using a Finnigan LCQ high performance liquid chromatograph/mass spectrometer (HPLC/MS). The gas phase samples were prepared by injecting 3 mL of headspace gas using a gas-tight syringe into a sealed vial containing 1 mL of methanol. Total organic carbon (TOC) concentrations were measured using a Shimadzu total organic carbon analyzer.

2.4 Quantum mechanical simulations

Density functional theory simulations were performed to investigate possible PFBS reaction mechanisms. DFT calculations were performed using the DMol3 [7, 8] package in the Accelrys Materials Studio [9] modeling suite using a personal computer. All simulations used double-numeric with polarization (DNP) basis sets [10] and the gradient

corrected Vosko-Wilk-Nusair-Becke-Perdew (VWN-BP) functionals for exchange and correlation [11–13]. The nuclei and core electrons were described by DFT optimized semi-local pseudopotentials [14]. Implicit solvation was incorporated into all simulations using the COSMO-ibs [15] model. This solvation model is particularly suited for reacting systems undergoing changes in atomic binding.

Transition state searches were performed using a quadratic synchronous transit (QST) method [16] and refined using an eigenvector following method as described in [17]. The energy optimized structures and transition states were verified by frequency calculations. Imaginary frequencies with wave numbers smaller than 10 cm^{-1} were considered numerical artifacts of the integration grid and convergence criteria [18, 19].

3 Results and discussion

Figure 1a shows PFBS and TOC concentrations as a function of electrolysis time at a current density of 10 mA cm^{-2} at 22 °C in the flow-through reactor. Figure 1b shows the sulfate and fluoride concentrations for the same experiment. The PFBS oxidation products consisted of carbon dioxide, sulfate, fluoride, and trace amounts of TFA. Throughout the course of the experiment, the only detectable organic reaction product was TFA which appeared at trace levels representing <3% of the PFBS removed. This indicates that >97% of the organic reaction products intermediate between PFBS and CO_2 did not re-enter the bulk solution, and either remained adsorbed to the electrode surface or remained sufficiently close to the electrode surface to undergo subsequent oxidation steps prior to partitioning back into the bulk solution. The near absence of intermediate reaction products in solution is confirmed by the close agreement between PFBS removal and TOC removal in Fig. 1a. Over the course of the experiments, solution pH values decreased from 5 to 3, indicating the production and subsequent hydrolysis of CO_2 to carbonic acid. The ratio of sulfate produced per PFBS removed was 1.0 ± 0.1, indicating a complete mass balance on sulfur atoms. Fluoride recovery averaged 8.2 ± 0.3 out of 9 fluoride ions per PFBS degraded. The average recovery of only 91% for fluoride may result from the loss of fluorinated species, such as HF and TFA, into the gas phase. Although the closed-loop system was gas-tight, headspace accounted for 60% of the volume in the feed water reservoir.

Experiments measuring PFBS oxidation kinetics were performed using a RDE operated at 3,000 rpm. At this rotation speed, diffusive mass transfer to the electrode surface was more than two orders of magnitude greater than the observed PFBS oxidation rates. Therefore, the measured reaction rates were not affected by the rate of

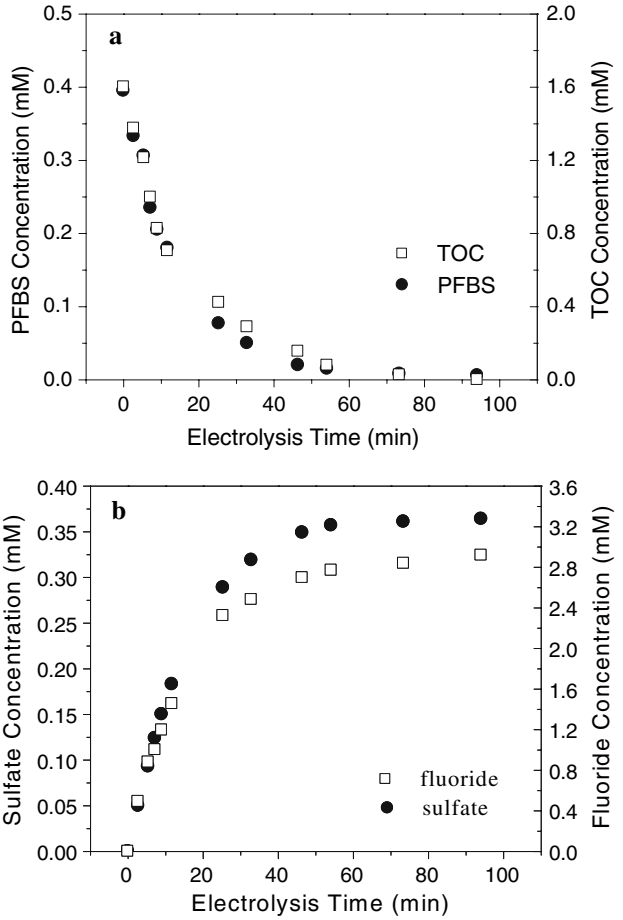

Fig. 1 **a** PFBS (*filled circle*) and TOC (*open square*) and **b** sulfate (*filled circle*) and fluoride (*open square*) concentrations as a function of electrolysis time at current a density of 10 mA cm^{-2} in the flow-through reactor

mass transfer to the electrode surface. Figure 2 shows PFBS concentrations in the RDE reactor at fixed current densities of 5, 10, 15, and 20 mA cm^{-2} at 22 °C. In all experiments, the oxidation rate of PFBS was zeroth order in PFBS concentration and increased with increasing current density. This type of behavior is typical for surface reactions whose rates are limited by the availability of reaction sites. TOC was removed at the same rate as PFBS in the RDE experiments. The slope of the regression line for TOC removed versus PFBS removed was 0.996. The average Faradaic current efficiency over the entire electrolysis period for the data in Fig. 2 ranged from 3.3% to 4.4%, based on 18 electrons per PFBS removed (2 per sulfur and 4 per carbon atom). This indicates that the predominant anode reaction was oxygen evolution.

Insight into the PFBS reaction mechanism may be gained by examining the apparent electron transfer coefficient ($\bar{\alpha}$) for PFBS oxidation, as illustrated in Fig. 3. For an ideal anodically polarized p-type semiconductor electrode,

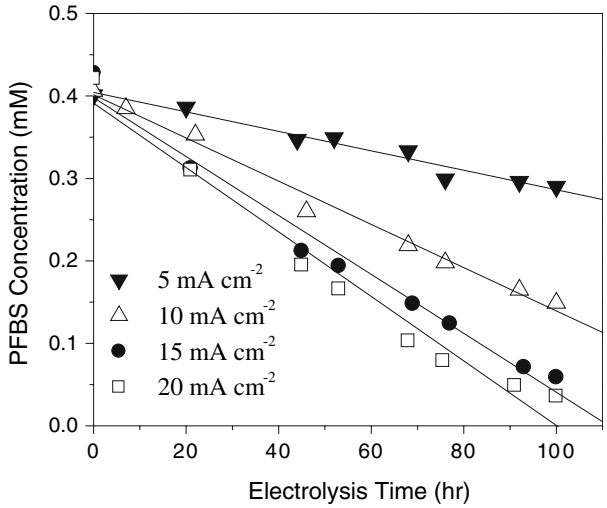

Fig. 2 PFBS concentration as a function of electrolysis time at current densities of 5 (*filled inverted triangle*), 10 (*open triangle*), 15 (*filled circle*), and 20 (*open square*) mA cm^{-2} in the RDE reactor

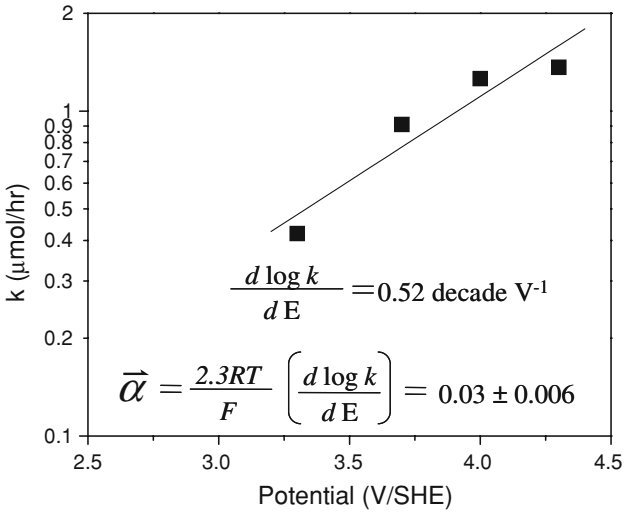

Fig. 3 PFBS rate constant in µmol h^{-1} as a function of the electrode potential. Also shown is the apparent electron transfer coefficient ($\bar{\alpha}$)

an electron transfer coefficient of 1 is expected [20]. However, heavily doped BDD electrodes have been found to show near metallic behavior [20]. In the case of metallic behavior, electron transfer coefficients near 0.5 are expected [20]. Figure 3 shows a plot of the logarithm of zeroth order rate constants as a function of the electrode potential. These data yield an electron transfer coefficient $\bar{\alpha} = 0.03 \pm 0.006$. The small value of the electron transfer coefficient indicates that PFBS reaction rates were only weakly dependent on the electrode potential. This behavior may be attributed to a reaction mechanism involving indirect oxidation by hydroxyl radicals produced from water oxidation, as proposed in previous investigations [21–26]. The weak potential dependence associated with oxidation by $HO^{\bullet}$ may arise because the concentration of hydroxyl radicals approaches a limiting value at electrode potentials approaching ~3 V/SHE [20, 21]. Alternatively, a weak potential dependence may arise in direct electron transfer reactions in regions where the overpotential is sufficiently high that available electronic energy states in the electrode are lower than those in the reacting species [20]. This situation produces an activationless barrier and the reaction rates become independent of the electrode potential.

The temperature dependence of the PFBS reaction rates can be used to gain insight into the rate-limiting step in the reaction mechanism. PFBS reaction rates measured at 7, 15, 22, 25, and 45 °C were used to determine the apparent activation energies for PFBS oxidation, as illustrated in the Eyring plot shown in Fig. 4. The data in Fig. 4 yield an apparent activation energy of only 9.3 ± 3 kJ mol^{-1}. Reactions with activation barriers this low generally proceed readily at room temperature [27].

Density functional theory simulations were performed to determine the activation barriers for the reaction of hydroxyl radicals at different sites on the PFBS molecule. Figure 5 shows the transition state and final product for hydroxyl radical attack at the $-SO_3^-$ group. The reaction produced HSO_4^- and a nonafluoro-1-butane radical with an overall reaction energy of −84 kJ mol^{-1}. The activation energy determined from the transition state was 123 kJ mol^{-1}. Hydroxyl radical activation barriers this high are generally associated with reactions that do not readily occur at room temperature [27]. For example, activation energies for $HO^{\bullet}$ reaction with perchlorinated biphenyls (PCBs) range from 71 to 93 kJ mol^{-1} [28, 29]. These high activation energies explain the lack of PCB

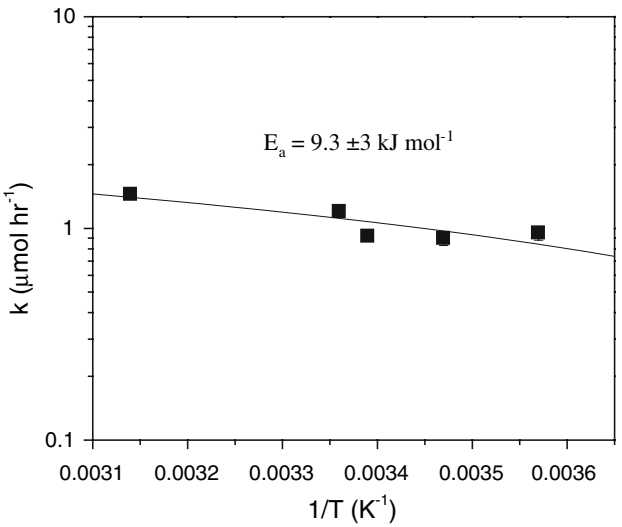

Fig. 4 Erying plot of zeroth order rate constants for PFBS oxidation at a fixed current density of 10 mA cm^{-2}

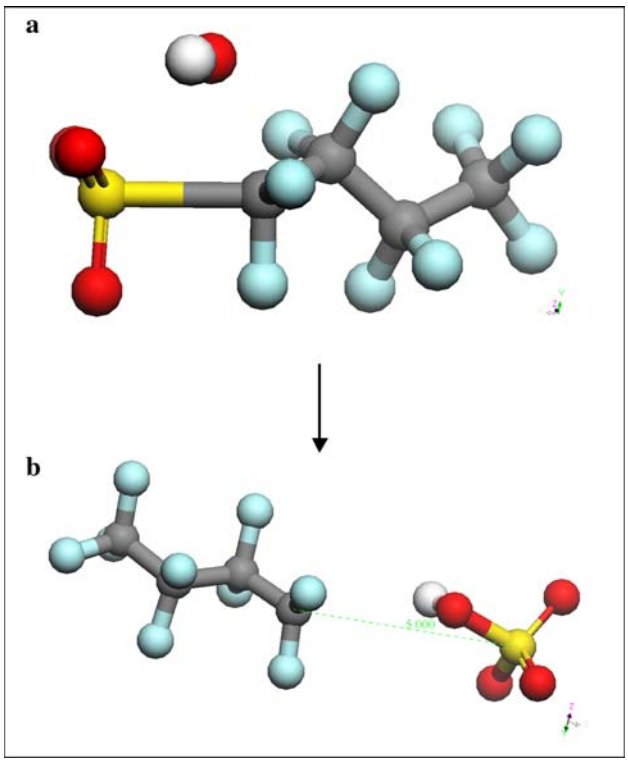

Fig. 5 Transition state (**a**) and final products (**b**) for hydroxyl radical attack at the $-SO_3^-$ group. Atom key: C-gray, F-blue, O-red, H-white, S-yellow

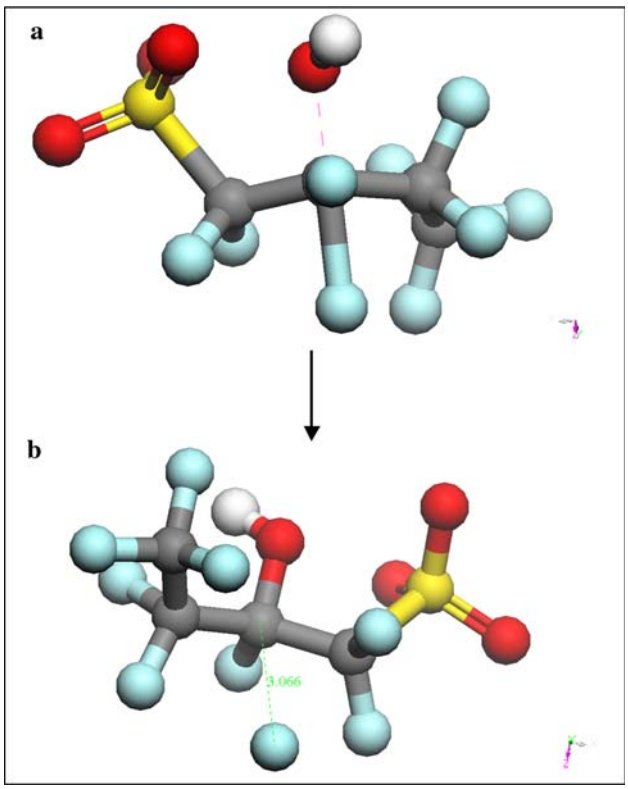

Fig. 6 Transition state (**a**) and final products (**b**) for replacement of a fluorine atom with hydroxyl radical. Atom key: C-gray, F-blue, O-red, H-white, S-yellow

oxidation by hydroxyl radicals at room temperature. In contrast, phenol, which readily reacts with hydroxyl radicals at room temperature, has activation barriers ranging from 4 to 25 kJ mol^{-1}, depending on the site of attack [30].

Activation energies for $HO^{\bullet}$ reaction at other sites on the PFBS molecule were also calculated. Figure 6 shows the transition state and final products for replacement of a fluorine atom with $HO^{\bullet}$. The reaction produces a fluoride ion and an octafluoro-1-butanesulfonate-2 hydroxyl carbon radical with an overall reaction energy of +70 kJ mol^{-1}. The activation barrier of 172 kJ mol^{-1} is much higher than that for attack at the $-SO_3^-$ site and is consistent with the high strength of carbon-fluorine bonds. Figure 7 shows the transition state and final products for attack of $HO^{\bullet}$ at one of the carbon-carbon bonds in PFBS. The reaction produced pentafluoroethanol and a tetrafluoro-ethanesulfonate radical with an overall reaction energy of −150 kJ mol^{-1}. The activation barrier for this reaction was 288 kJ mol^{-1}. The high activation barrier indicates that this reaction is not important in the oxidation pathway of PFBS.

The high activation barriers for PFBS oxidation by $HO^{\bullet}$ are consistent with the lack of reaction of perfluorinated alkyl sulfonates with AOPs employing hydroxyl radicals. For example, Schroder and Meesters [5] showed that there was no reaction of PFOS with hydrogen peroxide in combination with Fenton's reagent, ozone, or ultraviolet light. This finding suggests that the rate-limiting step for PFBS oxidation involves direct electron transfer.

Density functional theory simulations were used to determine the activation energies for direct oxidation of PFBS as a function of the electrode potential using the methods described in Anderson and Kang [31]. DFT simulations indicate that loss of one electron leads to lengthening of the C–S bond, and that the C–S bond length closely approximates the reaction coordinate (i.e., >90% of the energy change between the reactant and the transition state is due to C–S bond lengthening). Figure 8a shows the energy of the reactant (PFBS anion) and products (PFBS neutral radical + electron) as a function of the C–S bond length at a potential of 2.5 V/SHE. Product energies as a function of electrode potential were determined by shifting the energy profile of the product species downwards by 96.5 kJ mol^{-1} (i.e., 1.0 eV) to increase the electrode potential by 1.0 V and upwards by 96.5 kJ mol^{-1} to decrease the electrode potential by 1.0 V [31]. Electron energies from the vacuum scale were converted to the SHE scale by subtracting 4.6 eV [31]. The higher the electrode potential, the shorter the C–S bond stretching required for the reactant and product energy profiles to intersect. Intersection of the two energy profiles yields the bond

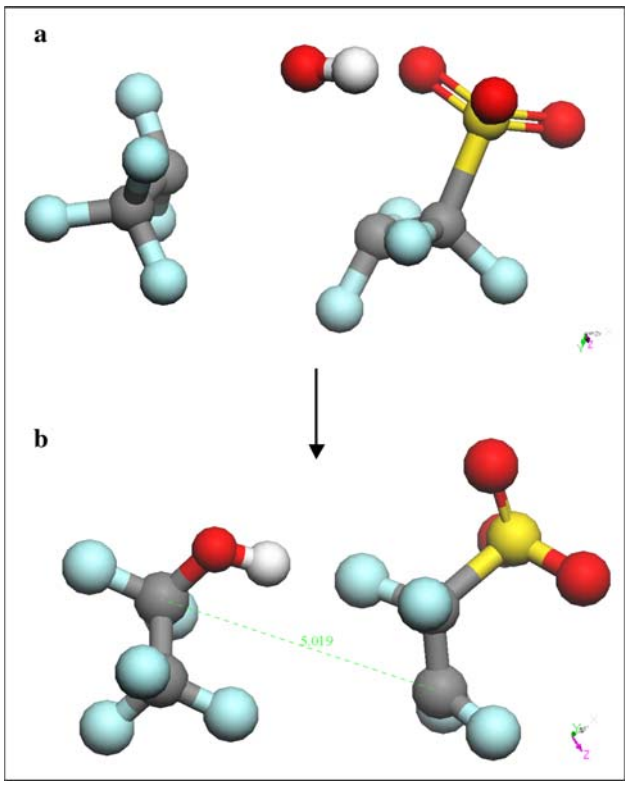

Fig. 7 Transition state (**a**) and final products (**b**) for hydroxyl radical attack at one of the carbon-carbon bonds. Atom key: C-gray, F-blue, O-red, H-white, S-yellow

length at the transition state and the activation energy for the reaction:

$$C_4F_9SO_3^- \rightarrow C_4F_9SO_3^{\bullet} + e^-. \quad (2)$$

By shifting the products energy profile up and down, activation energies as a function of electrode potential were calculated, as shown in Fig. 8b. Figure 8b shows that the activation energy decreases from 270 kJ mol^{-1} at a potential of 1.0 V/SHE to 0 at a potential of 3.0 V/SHE. This indicates that the reaction becomes activationless at potentials greater than 3.0 V/SHE and is consistent with the low apparent activation energy calculated in Fig. 4.

This study showed that PFBS can be readily oxidized at BDD electrodes while producing only trace amounts of organic products in the solution. The reaction occurs in the high overpotential region where there is activationless electron transfer. This occurs because the electrode is at a sufficiently high potential that there are unoccupied electron energy levels in the electrode that are lower than that for the highest occupied molecular orbital in PFBS. The DFT simulations show that with the transfer of the second electron, the C–S bond is cleaved. Mineralization of the PFBS residue likely occurs via a combination of direct electron transfer and reaction with hydroxyl radicals. The fact that intermediates between PFBS and carbon dioxide

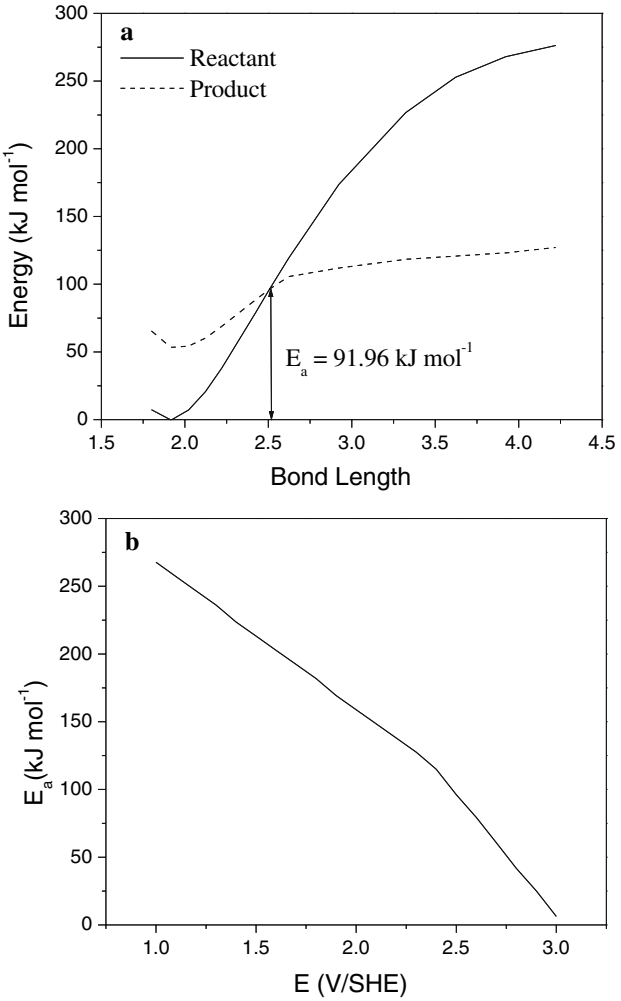

Fig. 8 **a** Energy profiles for reactant ($C_4F_9SO_3^-$) and products ($C_4F_9SO_3^{\bullet} + e^-$) for vertical electron transfer as a function of the C–S bond length at an electrode potential of 2.5 V/SHE. **b** Activation energies as a function of electrode potential for a direct electron transfer reaction

are not observed in the solution suggests that they are fast reacting and/or remain adsorbed to the electrode surface.

Acknowledgments We are grateful to the National Science Foundation Chemical and Transport Systems Directorate (CTS-0522790), and the Semiconductor Research Corporation/Sematech Engineering Research Center for Environmentally Benign Semiconductor Manufacturing (2001MC425), and the Donors of the American Chemical Society Petroleum Research Fund (PRF 43535-AC5) for support of this study.

References

1. Giesy JP, Kannan K (2001) Environ Sci Technol 35:1339
2. Organization for Economic Co-operation and Development (2002) Hazard assessment of perfluorooctane sulfonate (PFOS) and its salts. ENV/JM/RD (2002)17/FINAL. http://www.fluorideaction.org/pesticides/pfos.final.report.nov.2002.pdf

3. U.S. Environmental Protection Agency (2000) Fed Regist 65:62319
4. U.S. Environmental Protection Agency (2002) Fed Regist 67:326
5. Schroder HF, Meesters RJW (2005) J Chromatogr A 1082:110
6. Michaud PA, Panizza M, Ouattara L, Diaco T, Foti G, Comninellis Ch (2003) J Appl Electrochem 33:151
7. Delley B (1990) J Chem Phys 92:508
8. Delley B (2000) J Chem Phys 113:7756
9. Accelrys Corporation, Materials Studio, 4.2, San Diego, CA
10. Delley B (1996) J Phys Chem 100:6107
11. Vosko SH, Wilk L, Nusair M (1980) Can J Phys 58:1200
12. Becke AD (1988) J Chem Phys 88:2547
13. Perdew JP, Wang Y (1992) Phys Rev B 45:13244
14. Delley B (2002) Phys Rev B 66:155125
15. Delley B (2006) Mol Simulation 32:117
16. Halgren TA, Lipscomb WN (1977) Chem Phys Lett 49:225
17. Fischer S, Karplus M (1992) Chem Phys Lett 194:252
18. Barbosa LAM, Sautet P (2002) J Catal 207:127
19. Ochterski JW (2000) Vibrational analysis in Gaussian. Gaussian, Inc, Pittsburgh
20. Bockris JO'M, Reddy AKN, Gamboa-Aldeco M (2000) Modern electrochemistry, vol 2A, 2nd edn. Kluwer Academic, New York
21. Farrell J, Martin FJ, Martin HB, O'Grady WE, Natishan P (2005) J Electrochem Soc 152:E14
22. Tamilmani S, Huang WH, Raghavan S, Farrell J (2004) IEEE Trans Semicond Manuf 17:448
23. Marselli B, Garcia-Gomez J, Michaud PA, Rodrigo MA, Comninellis Ch (2003) J Electrochem Soc 150:D79
24. Zhu X, Shi S, Wei J, Lv F, Zhao H, Kong J, He Q, Ni J (2007) Environ Sci Technol 41:6541
25. Hagans PL, Natishan PM, Stoner BR, O'Grady WE (2001) J Electrochem Soc 148:E298
26. Iniesta I, Michaud PA, Panizza M, Cerisola G, Aldaz A, Comninellis Ch (2001) Electrochim Acta 46:3573
27. Wade LG Jr (1999) Organic chemistry, 4th edn. Prentice Hall, New York
28. Murena F, Schioppa E, Gioia F (2000) Environ Sci Technol 34:4382
29. Lin YJ, Chen YL, Huang CY, Wu MF (2006) J Hazard Mater 136:902
30. Wang Y, Liu Y, Luo Y, Zhang W, Zhong R (2006) Acta Phys-Chim Sin 22:1266
31. Anderson AF, Kang DB (1998) J Phys Chem A 102:5993